Original Article

The effect of combining Endostar with radiotherapy on blood vessels, tumor-associated macrophages, and T cells in brain metastases of Lewis lung cancer

Ling Peng[#], Ying Wang[#], Shihong Fei[#], Chunhua Wei, Fan Tong, Gang Wu, Hong Ma, Xiaorong Dong

Cancer Center, Union Hospital, Tongji Medical College, Huazhong University of Science and Technology, Wuhan 430022, China

Contributions: (I) Conception and design: H Ma, X Dong; (II) Administrative support: F Tong, G Wu; (III) Provision of study materials or patients: S Fei, C Wei; (IV) Collection and assembly of data: L Peng, Y Wang, S Fei; (V) Data analysis and interpretation: L Peng, Y Wang; (VI) Manuscript writing: All authors; (VII) Final approval of manuscript: All authors.

[#]These authors contributed equally to this work.

Correspondence to: Prof. Hong Ma; Prof. Xiaorong Dong. Cancer Center, Union Hospital, Tongji Medical College, Huazhong University of Science and Technology, Wuhan 430022, China. Email: wudajianzhu2004@163.com; xiaorongdong@hust.edu.cn.

Background: Combining Endostar (ES) with radiotherapy (RT) has shown a promising therapeutic effect on non-small cell lung carcinoma with brain metastases (BMs) in clinical practice. However, the specific mechanism is not yet fully understood. The present study aimed to investigate the effects of ES on blood vessels, tumor-associated macrophages (TAMs), and T cells in a tumor microenvironment treated with RT.

Methods: BM models were established by stereotactic and intracarotid injection of luciferase-Lewis lung cancer (LLC) cells into female C57BL mice. The animals were randomly divided into 4 groups: normal saline (NS), ES, RT, and ES plus radiotherapy (ES + RT) groups. Tumor size was determined with the IVIS imaging system. Tumor specimens were stained with CD34 and α-SMA to investigate tumor vascular changes. The proportions of TAMs, $CD4^+$ T cells, and $CD8^+$ T cells in tumor tissues were determined by flow cytometry and immunofluorescence. The expressions of hypoxia-inducible factor 1α (HIF-1α) and CXCR4 were deduced using western blotting and immunohistochemistry (IHC).

Results: ES + RT significantly suppressed tumor growth compared to the other 3 groups. RT decreased M1 and increased M2 in microglial cells and bone marrow-derived macrophages (BMDMs) relative to NS, while ES had the opposite effect. The ratio of $CD8^+$T/$CD4^+$T was increased in the ES + RT group compared to the other 3 groups. Tumor vascular maturity (α-SMA^+/$CD34^+$) was increased while HIF-1α was significantly suppressed in the ES + RT group. CXCR4 expression, which is involved in TAM recruitment, increased following RT, whereas, ES attenuated its expression.

Conclusions: Our findings suggest that ES can promote the normalization of tumor blood vessels and increase the anti-tumor immune-related immune cells infiltrating the tumor following RT treatment.

Keywords: Lung cancer; brain metastases (BMs); tumor-associated macrophages (TAMs); Endostar (ES); radiotherapy (RT).

Submitted Dec 23, 2019. Accepted for publication Jun 02, 2020.

doi: 10.21037/tlcr-20-500

View this article at: http://dx.doi.org/10.21037/tlcr-20-500

Introduction

Lung cancer persists as the deadliest cancer afflicting men and women worldwide (1). Nearly 80% of lung cancers are non-small cell lung cancer (NSCLC), making NSCLC the most common subtype (2). Among these cases, at least one-third of the people with lung cancer develop brain metastases (BMs) with radiotherapy (RT) being the primary therapy for this metastasis type (3).Even though the development of clinical technology has made RT more efficient, local failures still occur in a significant portion of patients (4). Studies have found that hypoxia-inducible factor 1α (HIF-1α) independently promotes radioresistance (5), while other preclinical evidence indicates that vascular endothelial growth factor (VEGF) being reactively upregulated in tumors from RT might be a contributor to the development of radioresistance (6). One probable route for radioresistance could be the activation of the PI3K/Akt/mTOR pathway which in turn helps activate the HIF-1α-VEGF pathway in tumor cells (7). Most recently, it was confirmed that tumor-associated macrophages (TAMs) could drive tumor regrowth after local RT (8), and there is strong evidence that tumor infiltration by TAMs is associated with poor patient prognosis for many types of cancers (9-13). TAMs, including microglia, are the most prevalent immune cells in tumors and are predominantly M2-like with immunosuppressive and angiogenic properties (14). Studies have suggested that hypoxia induces significant M2 polarization of macrophages in tumors (15). Therefore, promoting blood vessels to improve hypoxia and tumor microenvironment is a critical path to reduce RT resistance.

One avenue of present research involves normalizing vessels to increase the response to RT and decrease tumor metastasis and recurrence. Vascular normalization arises when an imbalance of anti-angiogenesis and pro-angiogenesis factors in the tumor microenvironment recover to baseline levels. This process consists of increasing pericyte coverage of endothelial cells and decreasing vessel dilatation, which can improve tumor perfusion and oxygenation (16). The opportunity for normalization, combined with pro-angiogenesis induced by irradiation signaling, is the clinical rationale behind coupling anti-angiogenesis therapy with RT (17,18).

Endostatin is a global inhibitor of endothelial cell proliferation *in vitro* and angiogenesis *in vivo*. Human recombinant endostatin [Endostar (ES)] has been given approval by the State Food and Drug Administration (FDA) to treat patients with non-small cell lung cancer in China. Clinical trials have shown ES to be most effective when combined with other therapies, including radiotherapies. Prior research suggests that ES is capable of effectively blocking angiogenesis and normalizing tumor vasculature in many cancer types (19). Other investigations have demonstrated endostatin have an indirect or direct effect on immune cells. For instance, Rocha *et al.* discovered that, in the tumors of mice, extensive leukocyte infiltration could be induced by endostatin gene therapy (20). Still other studies have revealed that treating with endostatin increases the infiltration levels of cytotoxic lymphocytes, including natural killer cells and $CD8^+$ cells, implicating endostatin as a promoter of T cell activity, while radiotherapy facilitates proliferation of $CD4^+$ to Tregs and inducts the apoptosis in $CD8^+$ cytotoxic lymphocytes. CXCR4, along with its ligand, CXCL12, contributes to tumor angiogenesis, directional metastasis, and cancer-related chemo- and RT resistance (21). CXCR4, which participates in TAM recruitment, also plays a critical role in RT (22), and ES has been found to markedly reduce CXCR4 expression (23).

In this study, we hypothesized that ES could optimize the impact of RT through blocking RT-induced CXCR4 and subsequently suppressing TAM infiltration and M2-polarization. Contemporary research has elucidated the nature of the radiotherapeutic effects on vascular cells and the significance of maintaining a dose schedule in dual-modality treatment. The goal of the present study was to verify the effect of the combined use of ES with RT on blood vessels, TAMs, and T cells in BMs of Lewis lung cancer (LLC).

We present the following article in accordance with the ARRIVE reporting checklist (available at http://dx.doi.org/10.21037/tlcr-20-500).

Methods

Lewis lung cancer cell line used in our experiment were purchased by Huazhong University of Science and Technology (Wuhan, China) from the Cell Bank of the Chinese Academy of Sciences and propagated in DMEM medium (Gibco, Grand Island, NY, USA) supplemented with 10% fetal bovine serum (Gibco) and antibiotics (100 units/mL penicillin and 100 μg/mL streptomycin). The human recombinant endostatin, Endostar (rh-ES), was kindly provided by Shandong Simcere Medgenn Biopharmaceutical Co. (Yantai, Shandong, China) and stored at 4 ℃.

Antibodies

Antibodies used in this study included rabbit anti-mouse CD34 antibody (boster; catalog no. BM0532), mouse anti-mouseα-SMA antibody (boster; catalog no. BM0002), rabbit anti-mouse CD206 antibody (abcam; catalog no. ab64693), mouse anti-mouse CD86 antibody (abcam; catalog no. 213044), rabbit anti-mouse Iba-1 antibody (WAKO; catalog no. 019-19741), rabbit anti-mouse iNOS antibody (Abcam; catalog no. 15323), rabbit anti-mouse Arg-1 antibody (Proteintech; catalog no. AP16001), mouse anti-CXCR4 antibody (Proteintech; catalog no. 60042-1-Ig), rabbit anti-mouse VEGF antibody (Proteintech; catalog no.19003-1-AP), FITC anti-mouse CD3ε antibody (Biolegend; catalog no. 100306), APC/Cy7 anti-mouse CD4 antibody (Biolegend; catalog no. 100526), PE anti-mouse CD8a antibody (Biolegend; catalog no. 100708), FITC anti-mouse/human CD11b antibody (Biolegend; catalog no. 101206); PerCP anti-mouse CD45 antibody (biolegend; catalog no. 103130), PE anti-mouse CD86 antibody (biolegend; catalog no. 105008), PE/Cy7 anti-mouse CD206 (MMR) antibody (biolegend; catalog no. 141720), APC anti-mouse F4/80 antibody (biolegend; catalog no.123116), Cy3-conjugated goat anti-mouse antibody (Servicebio; catalog no. GB21301), FITC-conjugated goat anti-rabbit antibody (Servicebio; catalog no. GB22303), FITC-conjugated goat anti-mouse antibody (Servicebio; catalog no. GB22301), and Cy3-conjugated goat anti-rabbit antibody (Servicebio; catalog no. GB21303).

In vivo model of brain metastasis

All experiments were performed under a project license (license number S2326) granted by the Institutional Animal Care and Use Committee at Tongji Medical College, Huazhong University of Science and Technology, in compliance with institutional guidelines for the care and use of animals. We attempted to minimize the quantity of specimens needed and the suffering of the animals in the experiments.

C57BL/C mice can easily form tumors after incubation of cancer cells by stereotactic injection or intracarotid injection model (24,25). And it is immunocompetent animals that they have been used to study interactions between metastatic tumor cells and the host microenvironment (26,27). Female C57BL mice, aged 6–8 weeks, were bought from the Liaoning Changsheng Bioscience Company (Liaoning, China) and housed under monitoring in an environment free of pathogens. An *in vivo* model of brain metastasis was created as done in prior studies, with tumor cells [2×10^5 in 0.1 mL phosphate-buffered saline (PBS)] being gradually injected into the intracarotid artery of the C57BL mice (28).

Stereotactic intracranial transplantation models were created as follows. After anesthetizing mice with pentobarbital sodium, their crania were exposed by incision, and small holes were drilled 2.5 mm lateral and 0.5 mm anterior to the bregma using a size 34 inverted cone burr. Each mouse was then positioned in a stereotactic frame, and 1×10^5 cells in 5 μL PBS were slowly injected into the right striatum 3 mm below the dura mater using a 27-gauge needle. The incision was closed with a 5-0 silk at the end of transplantation.

Bioluminescence imaging of in vivo model of brain metastasis, drugs administration and tumor irradiation

Tumor bioluminescence were viable for detection by the IVIS imaging system after 6 days' incubation of LLC cells in orthotopic brain transplantation model and 14 days' incubation of LLC cells in intracarotid injection model using an IVIS Spectrum scanner (Bruker, USA). A D-luciferin potassium salt solution (Goldbio. St. Louis, MO, USA) was injected intraperitoneally (150 mg/kg), and imaging of the mice continued until peak radiance could be acquired. Living Image Software (Bruker MI, USA) was used to measure the total flux of a brain tumor in automatically selected regions of interest.

The transplanted mice were divided into 4 groups (n=6 mice for each group) using random number table and random number remainder grouping: the normal saline (NS), ES, RT, and ES plus radiotherapy (ES + RT) groups. NS (0.1 mL) was given to mice in the NS and RT groups, while ES (15 mg/kg) was administered to mice in the ES and ES + RT groups for 14 days by intraperitoneal injection. And the day was set as day 1 when mice was grouped and treated. Mice in the RT and ES + RT groups were subjected to 10 Gy irradiation on day 7 after tumor bioluminescence imaging. Irradiation was administered with a Varian Clinac 600C X-ray unit at 250 cGy/min (80 cm source-to-skin distance). Prior to irradiation, anesthesia of 1% pentobarbital sodium was applied to all mice, and irradiation proceeded with a protective lead cover, and only the whole brain being exposed to the field. Mice brains were removed after tumor bioluminescence were detected on day 14. Fresh brain (six mice each group)

were detected by flow cytometry or stored in –80 ℃ for western blotting. Some brains (six mice each group) were subsequently sectioned into pieces of 5 mm sections for histopathologically detection

Immunohistochemical and immunofluorescence stainings and vessels staining

Protein expression was determined by immunohistochemistry (IHC). Briefly, 5-μm serial sections of tumor tissues were dewaxed in xylene and rehydrated through graded alcohols. Endogenous peroxidases were blocked (3% H_2O_2, 30 min), and antigens were retrieved through microwaving the slides. They were cooled and washed, and then blocked with goat serum for 30 min. This was followed by tissue section incubation with primary antibodies at 4 ℃ overnight, and a subsequent incubation with HRP-conjugated secondary antibodies. Finally, the slides were stained by the Liquid DAB Substrate Chromogen System.

For immunofluorescent staining, after dewaxing and rehydrating tumor samples and retrieving and blocking antigens, tumor sections were stained with primary antibodies at 4 ℃ overnight and then incubated with FITC or Cy3-labeled secondary antibodies. Nuclei were stained with 10 μM DAPI. Cover slides were mounted using the Fluoromount-GTM medium, and tissue sections were observed with fluorescence microscopy.

To observe the leakage of blood vessels, each mouse was anesthetized and intravenously injected with 100 μL of 5 mg/mL 55–80 KD rhodamine-conjugated dextran (Sigma, USA), 2,000 KD FITC-conjugated dextran (Sigma, USA), and Hoechst 33342 (Sigma, USA) via the tail vein at the experimental endpoints after treatment. Twenty minutes after injection, animals were sacrificed, and their brains were removed and placed in 4% paraformaldehyde for 48 h and then placed in 30% sucrose for another 48 h. The brains were next frozen and cut into 10-μm slices. The integrity of each tumor was examined and compared against the other tumors under a fluorescence microscope.

Flow cytometry

Mononuclear cells were separated from the central nervous system (CNS) of mice using standard methods in the field, as described previously (29). Briefly, perfusion of the mice proceeded intracardially with PBS, and the whole brains of metastases models and brain tumors of stereotactic intracranial transplantation models were extracted and homogenized. Mononuclear cells were isolated by 25% discontinuous Percoll gradients (Sigma, St. Louis, MO, USA). The purified cells were stained with FITC anti-mouse CD3ε antibody, APC/Cy7 anti-mouse CD4 antibody, PE anti-mouse CD8a antibody, FITC anti-mouse/human CD11b antibody, PerCP anti-mouse CD45 antibody, PE anti-mouse CD86 antibody, PE/Cy7 anti-mouse CD206 (MMR) antibody, APC anti-mouse F4/80 antibody, and BV421-Zombie Violet Fixable Viability Kit (Biolegend). Fc receptors (FcR) were blocked with anti-mouse CD16/32. Antibody incubations were performed on ice, with the cells being fixed in 1% paraformaldehyde and analyzed on a BD LSRFortessa (BD Bioscience). The percentages of microglial cells and macrophages were obtained through counting the mean total number of mononuclear cells isolated from the CNS per mouse. Populations of $CD11b^{+}CD45^{low}$ $F4/80^{+}$-activated microglial cells and $CD11b^{+}CD45^{high}$ $F4/80^{+}$ peripheral macrophages were analyzed.

Statistical analysis

Unpaired two-tailed Student *t*-test and one-way analysis of variance (ANOVA) calculated the intergroup comparisons. All statistical analyses were conducted using SPSS (version 22.0) and GraphPad (Version 7.0). All data are presented as mean ± SD (standard deviation), and statistical significance was set as a P value <0.05.

Results

Combining ES and RT effectively inhibits tumor growth in orthotopic brain transplantation models and metastases models of LLC

The orthotopic brain transplantation models and intracarotid injection metastases models of LLC tumors were employed to determine whether the combination of ES and RT could improve anticancer effects. The mice were given NS, RT (10 Gy), ES (15 mg/kg per), or ES + RT when tumors were most viable for detection by the IVIS imaging system. The total quantified flux (six mice each group) on day 14 after treatment was collected for statistical analysis. The representative IVIS images of orthotopic brain transplantation tumor-bearing mice was shown (*Figure 1A*), and the representative IVIS images of intracarotid injection tumor-bearing mice was shown (*Figure 1B*). Compared to the control in both brain tumor models,

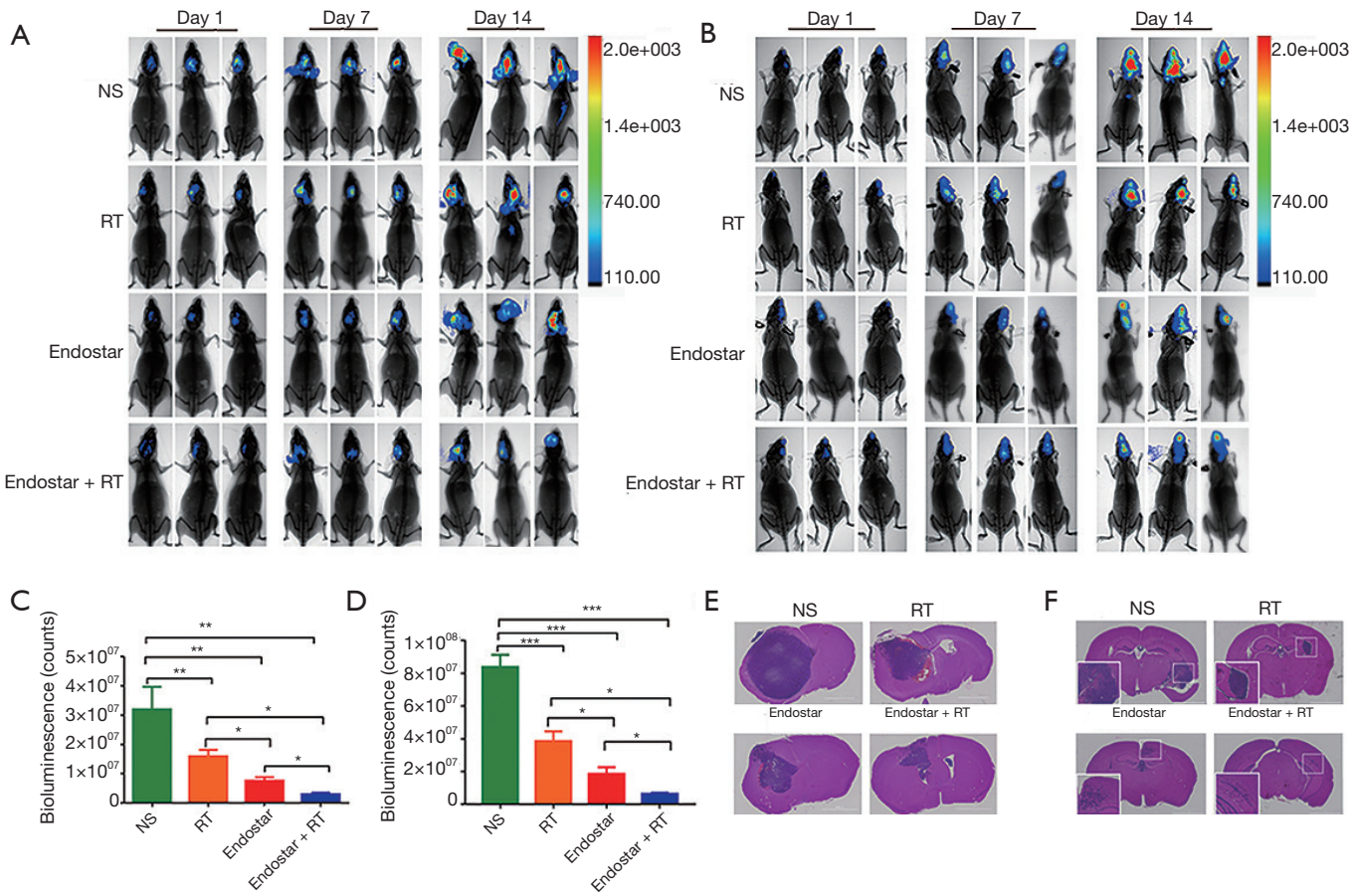

Figure 1 Combining Endostar with radiation therapy effectively inhibits tumor growth. LLC brain metastatic tumors were treated with NS, RT (10 Gy), ES (15 mg/kg per dose), or both (ES + RT). Quantification of the *in vivo* imaging system imaging data indicates tumor burdens. (A,B) *In vivo* bioluminescent images of orthotopic brain transplantation mice and intracarotid injection mice on days 1, 7, and 14 of NS, RT, ES, and ES + RT; (C,D) total quantified flux on day 14 after treatment with NS, RT, ES, and ES + RT in orthotopic transplantation mice and intracarotid injection mice. Results are represented as mean ± SD from 6 tumors per experimental group, P value as indicated, one-way ANOVA. *, P<0.05; **, P<0.01; ***, P<0.001; (E,F) HE staining results of orthotopic brain transplantation mice (scale =2,000 μm) (E) and intracarotid injection mice (scale =2,000 μm) (F) on day 14 after treatment of NS, RT, ES, and ES + RT. H&E, hematoxylin and eosin staining.

mice that received radiation or ES had reduced tumor bioluminescence on day 14 after treatment (P<0.01) (*Figure 1C,D*), whereas those treated with ES + RT had more diminished tumor bioluminescence (P<0.01) (*Figure 1C,D*). Moreover, the tumor bioluminescence of both brain tumor-bearing models in the ES + RT group was less than that of the mice in the radiation and ES groups (P<0.05) (*Figure 1C,D*). Thus, combining ES and RT cooperatively inhibits tumor progression.

Tumor tissues (six mice each group) were collected for hematoxylin and eosin (H&E) staining on day 14 after treatment. The combined therapy group displayed less necrosis in tumor sections compared to those of other groups in orthotopic brain transplantation models (*Figure 1E*). In the intracarotid injection tumor-bearing mice, microscopic lesions could be seen with HE staining. Meanwhile, multiple lesions could be seen on the whole-mount coronal section, and high-magnification images were characterized by diffuse or cluster type lesions (*Figure 1F*). Metastatic lesions appeared in either the parenchyma or leptomeninges of the CNS or both locations through the intracarotid injection approach (*Figure 1F*). The tumor area observed was the smallest in the combined group (*Figure 1F*).

Combining ES and RT changes tumor microvessel density and promotes vascular normalization

On day 14 after treatment, the mice (six mice each group)

were sacrificed, and tumors were collected for IHC analysis. An array of tests was used to determine if vessels were normalized, while CD34(endothelial cell marker) and α-SMA (α-smooth muscle action, pericyte coverage marker) staining was used to find vessels covered with pericytes. The analysis of tumor vasculature in orthotopic brain transplantation models revealed that tumors treated with RT, ES, and ES + RT in particular, had decreased $CD34^+$ blood vessel density compared with controls (*Figure 2A*). Moreover, pericyte coverage are important parameters for vessel maturation and functionality. In ES and ES + RT groups, vessels are lined with more mature α-SMA + pericyte cells compared with NS groups (*Figure 2A*). In intracarotid injection tumor-bearing mice, CD34 showed that tumor vessels were surrounded by tumor cell cluster (*Figure 2B*). The vessels were more regular and pericyte coverage were increased slightly in ES and ES + RT groups compared with NS and RT groups (*Figure 2B*). This result indicates that, ES alone exhibit an antiangiogenic effect and mitigate tumor vessel abnormality, and combining ES with RT has the most effect.

The blood-brain barrier is a physiological barrier that blocks more than 98% of small (>400 Da) and large molecule drugs from entering the CNS. The blood vessel in a tumor is malformed and characterized by rapid leakage. To address the question of whether the observed vascular remodeling also changes blood perfusion and vascular permeability, mice (six mice each group) were injected with FITC-conjugated dextran 2,000 KD, rhodamine-conjugated dextran 55–75 KD, and Hoechst 33342 on 14 day after treatment. The large molecule FITC-conjugated dextran (2,000 KD, green) was used to show perfusion. The small molecule rhodamine-conjugated dextran (55–75 KD, red) which could extravasate into the extravascular space through "leaky" tumor vessels was used to demonstrate leakage. Hoechst 33342 can pass through the cell membrane and is primarily used for cell labeling to show the tumor area. Based on the fluorescence imaging in the merged column, rhodamine-conjugated dextran extravasates into extravascular space through "leaky" tumor vessels in NS group in orthotopic brain transplantation models (*Figure 2C*). RT group changes were not apparent in comparison to ES group changes, whereas the red area decreased evidently in the ES + RT group in comparison to ES group and RT group in orthotopic brain transplantation tumor-bearing mice in (*Figure 2C*). In the intracarotid injection tumor-bearing mice, the red area that extravasates into extravascular space is reduced in ES + RT group in comparison to other three groups, whereas RT group changes were not apparent in comparison to NS group changes (*Figure 2D*). Overall, ES treatment improved vessel maturity, reducing vascular leakiness in brain tumors.

Combining ES and RT changes the number and phenotype of TAM from M2 to M1

Microglial cells of the CNS are present in a resting state and can be distinguished by their ramified and a $CD45^{low}$ expression pattern. Microglial cells have an immediate and diverse morphologic response to alterations in brain physiology along a continuum of possibilities that range from hyper-ramification and highly complex morphologies to de-ramified and amoeboid morphologies. Microglial cells may also become polarized and rod-shaped when the CNS is inflamed, and seem to mimic the phenotypic and morphologic characteristics of peripheral macrophages that migrate into the CNS in the reaction to inflammation. During tumor development, a subpopulation of microglial cells was observed being activated in the CNS and acquiring markers of both M1 and M2 phenotypes.

We studied the effect of different therapies on tumor TAM infiltration number and their phenotype. Subpopulations of TAM cells (six mice each group) were analyzed by IHC on day 14 after treatment in both models. As determined by IHC, microglial cells were increased in tumor area compared with normal brain, and the microglial cells were activated with de-ramified and amoeboid morphologies (*Figure 3A*). In the IHC sections of tumors from mice in both models, after treatment with RT, we observed an increase in Iba-1^+ macrophage (microglial cells) infiltration, compared to the other groups on day 14 after treatment (*Figure 3A*).

Additionally, Arg-1 M2-like TAM levels were increased slightly in RT groups compared with NS groups, whereas $CD86^+$ M1-like TAM levels were increased slightly in ES groups in orthotopic brain transplantation tumor-bearing mice on day 14 after treatment (*Figure 3B* left). This result indicates that, ES could mitigate M2-like TAM increase induced by RT and promote TAM reprogramming from M2 to M1.

In intracarotid injection tumor-bearing mice, we observed an increase in Arg-1 M2-like TAM levels and a decrease in $CD86^+$ M1-like TAM levels in RT group, compared to NS groups (*Figure 3B* right). However, this change could be reversed by ES (*Figure 3B* right).

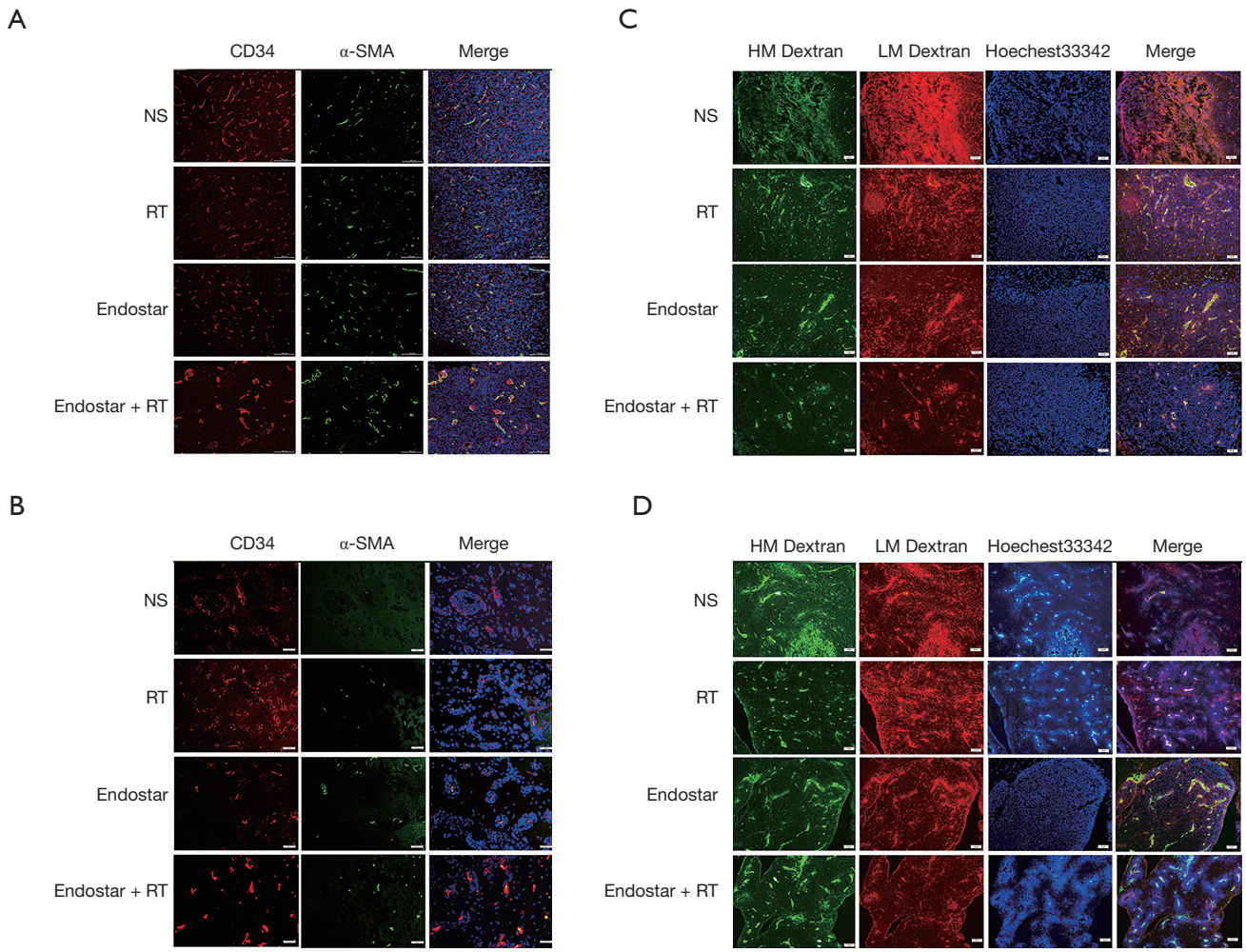

Figure 2 Endostar normalized the blood vessels of brain metastasis. (A) Representative images of CD34-positive endothelial cells and α-SMA pericyte-covered cells in tumor tissues of orthotopic brain transplantation mice on day 14 after treatment (scale =100 μm); (B) representative images of CD34-positive endothelial cells and α-SMA pericyte-covered cells in tumor tissues of intracarotid injection mice on days 14 after treatment (scale =20 μm); (C,D) two weeks after treatments, FITC-conjugated dextran (2,000 KD, green), rhodamine-conjugated dextran (55–75 KD, red), and Hoechst 33342 (blue) were injected into orthotopic brain transplantation mice and intracarotid injection mice for visualization of the blood vessels perfusion and vascular permeability (scale =20 μm). Based on the fluorescence imaging in the merged diagram, the overlapped areas of the green represent the actual range of blood vessels, while the separate red spots out of green denote the range of blood vessel leakage. Hoechst 33342 shows the areas of tumor tissue. α-SMA, α-Smooth muscle action.

Flow cytometry revealed that combining ES and RT changes TAM phenotype and T cells in brain tumor

TAMs are derived from circulating bone marrow-derived macrophages (BMDMs) and the microglial cells in brain tumors. Multiple models of murine brain malignancy and genetic lineage tracing have demonstrated that BMDMs are abundant in primary and metastatic brain tumors. Reportedly, >90% of macrophages in resistant tumors are bone marrow-derived. We therefore examined the origin of macrophages that become enriched in tumor microenvironments. Analyzing the expression profiles of the CD11b and CD45 markers using flow cytometry enabled us to discriminate between microglial cells ($CD11b^{+}CD45^{low}$) and BMDMs ($CD11b^{+}CD45^{high}$), as described by studies (29,30). TAMs represent multiple polarized immune cells mainly containing $F4/80^{+}CD86^{+}$ antitumoral M1 macrophages and $F4/80^{+}CD206^{+}$ protumoral M2

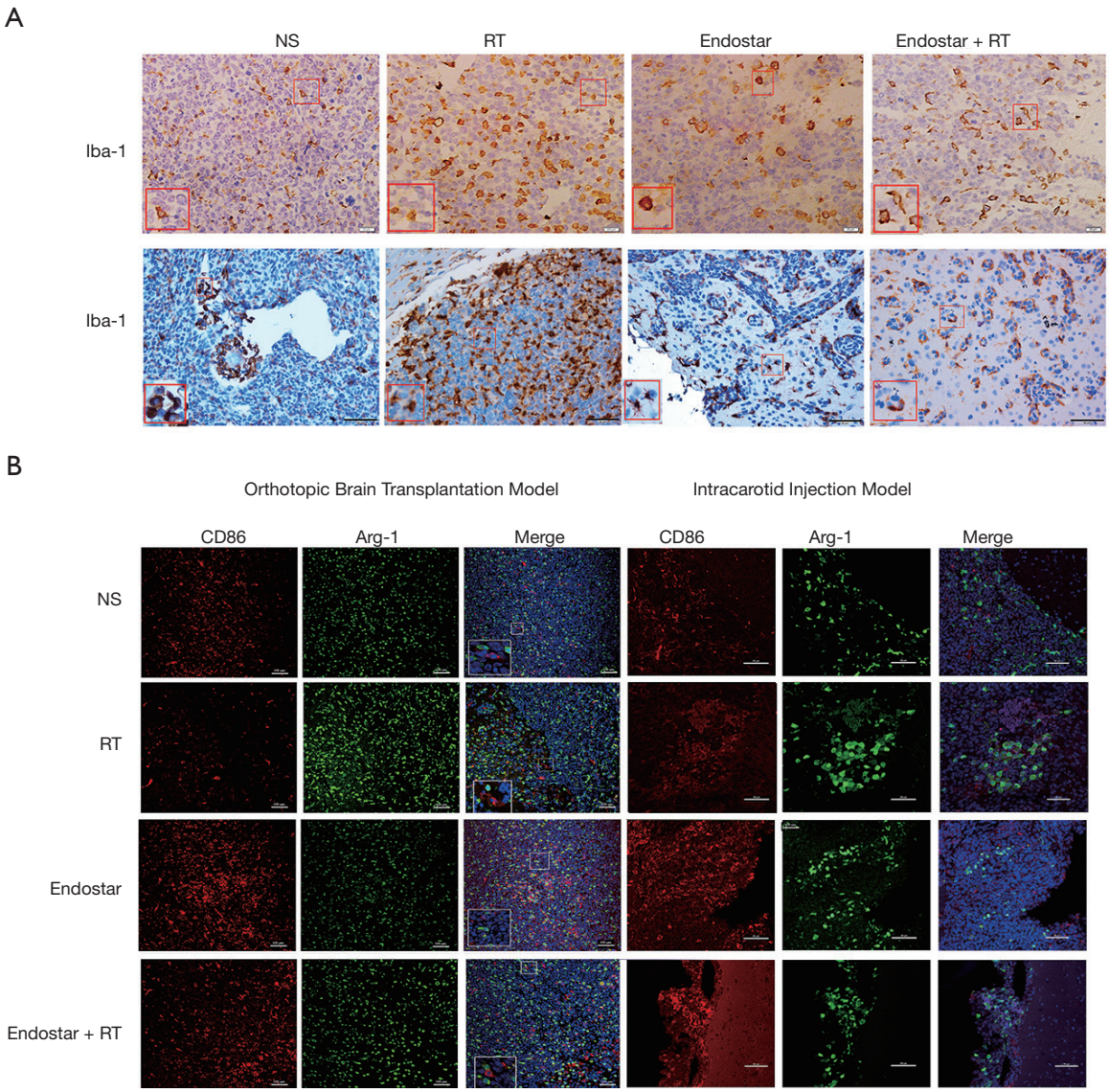

Figure 3 Combining Endostar with radiotherapy can reverse the decrease in the M1/M2 macrophage ratio induced by radiotherapy. (A) The microglial cells marker, Iba-1, were detected by IHC in the orthotopic transplantation model (top) (scale =20 μm) and intracarotid injection model (bottom) (scale =50 μm) on day 14 after treatment; (B) immunofluorescence co-staining of the M1 index CD86 and M2 index Arg-1 in the orthotopic transplantation model (left) and intracarotid injection model (right) on day 14 after treatment. (original magnification scale =100 μm on the left and scale =50 μm on the right). Iba-1, Ionized calcium-binding adaptor molecule-1.

macrophages (31,32). Representative gates (six mouse each group) for microglial cells and BMDMs of stereotactic injection model on day 14 after treatment were shown (*Figure 4A*). More than 75% of macrophages in tumors were microglial cells in orthotopic brain transplantation model, while only 45–50% were microglial cells in intracarotid injection models (*Figure 4B*). The proportion of microglial cells were increased in RT group compared with ES group in both models (P<0.05) (*Figure 4B*). Mice treated with ES were found to have a decreased amount of microglial cells with M2 phenotype markers relative to the RT group in intracarotid injection tumor-bearing mice models (P<0.05) (*Figure 4B*). Less than 20% of macrophages were BMDMs in orthotopic brain transplantation models, while 45–50% in intracarotid injection tumor-bearing mice (*Figure 4B*). The proportion of BMDMs were decreased

in RT group compared with ES group in intracarotid injection tumor-bearing mice models (P<0.05) (*Figure 4B*). We used mean fluorescence intensity (MFI) to determine the values of the M1/M2 markers within the BMDMs gate (*Figure 4C*), because the frequency of BMDMs is lower in the intracarotid injection model. Mice treated with ES were found to have a increased MFI of BMDMs with M1 phenotype markers relative to the NS group in BMDMs in intracarotid injection models (P<0.01) (*Figure 4C*). Meanwhile, mice treated with RT were found to have an increased MFI of BMDMs with M2 phenotype markers relative to the NS and ES group in intracarotid injection models (P<0.05) (*Figure 4C*). The ratio of BMDMs of the M1 phenotype to the M2 phenotype increased after ES treatment but diminished after RT in intracarotid injection models (P<0.05) (*Figure 4C*).

Representative gates (six mouse each group) for $CD4^+$ and $CD8^+$ T cells of stereotactic injection model on day 14 after treatment were shown (*Figure 5A*). The number of $CD4^+$ T cells was reduced (P<0.05) (*Figure 5B*), while the number of $CD8^+$ T cells was elevated after any treatment in the stereotactic injection model on day 14 after treatment (*Figure 5B*). Furthermore, the ratio of $CD8^+$ T cells to $CD4^+$ T cells increased markedly in the combination group (P<0.05) (*Figure 5B*). There was no statistical significance in tumor infiltrating T cell changes in intracarotid injection tumor-bearing mice models (*Figure 5C,D*). There was, however, no statistical significance in T cell changes in the blood in both models (data not shown).

ES-attenuated RT-induced CXCR4 is involved in TAM recruitment

HIF-1α, CXCR4, iNOS of orthotopic brain transplantation models (six mouse each group) were detected by Western blotting (WB) on day 14 after treatment (*Figure 6A*). WB showed that in contrast to NS treatment, HIF-1α levels post-RT, ES or ES + RT were markedly decreased (P<0.05) (*Figure 6B*). CXCR4 expression increased in response to radiation but were attenuated by ES (P<0.05) (*Figure 6B*). Compared to NS, ES enhanced the M1 phenotype macrophage population measured by iNOS, while radiation decreased the amount of these cells (P<0.05) (*Figure 6B*).

VEGF, HIF-1α, CXCR4 of orthotopic brain transplantation models were detected by IHC on day 14 after treatment. Results showed that in contrast with the NS group, the VEGF level of the other groups decreased. HIF-1α expression lessened in the ES and ES + RT groups in comparison to the NS group. CXCR4 expression increased in response to radiation but was attenuated by ES in the brain metastasis tumor models (*Figure 6C*).

Discussion

In 1971, Judah Folkman proposed that tumor growth is critically dependent upon neovascularization to supply itself with nutrients (33). A major abnormality of these tumor vessels lies in their atypical structure and function likely caused by an imbalance of pro- and antiangiogenic signals. Tumor blood vessels consist of irregular branches with arteriovenous shunts, which are absent in pericyte coverage and are highly permeable to plasma and plasma proteins (34). This condition gives rise to an atypical microenvironment with characteristic hypoxia, acidosis, and higher fluid pressure, all which in turn contribute to the tumor progressing, the treatment being resisted, and the proangiogenic growth factors in tumors being triggered (35).

Vascular damage caused by radiation strengthens tumor hypoxia and provokes immune responses via the elevated production of cytokines/chemokines that recruit immune cells (36). TAM is a key component of the tumor microenvironment and accounts for as high 50% of the tumor mass (37). Macrophages can be divided into anti-tumor M1 and pro-tumor M2, but being extremely plastic, their polarization balance is switchable. TAMs are absorbed into the tumor mass following RT with their main treatment-resistant contribution being characterized by the stimulation of angiogenesis and a release of growth factors (8) which, in turn, promote metastasis and tumor relapse after irradiation. The recruitment of TAMs has associations with a worse prognosis across a variety of cancers (38). Given this, a great deal of research has concerned itself with disrupting TAM recruitment and M2 polarization with the aim of enhancing anticancer treatment. Following RT, the comparable rise in the number of locally suppressive cell types, having a lower radio-sensitivity than other types of lymphocytes, is counteracted by the influx of circulating immune cells and elevated antigen exposure and presentation. Thus, modulating TAMs could be another way to curb tumor neovascularization.

The present study evaluated how TAMs were phenotypically repolarized from M2 to M1 when induced by combined ES and RT treatment of LLC cancer. We also assessed the effect of the combined therapy on tumor blood vessels. Pro-tumor M2 macrophages reduce the cytotoxic activity of immune cells by secreting factors

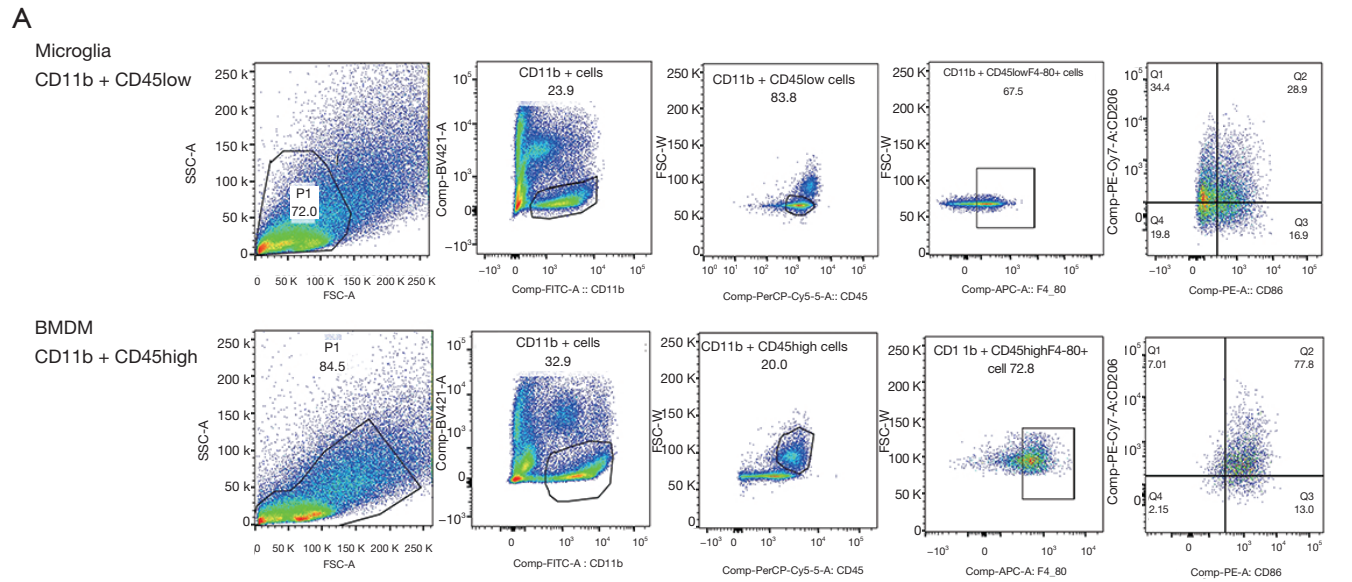

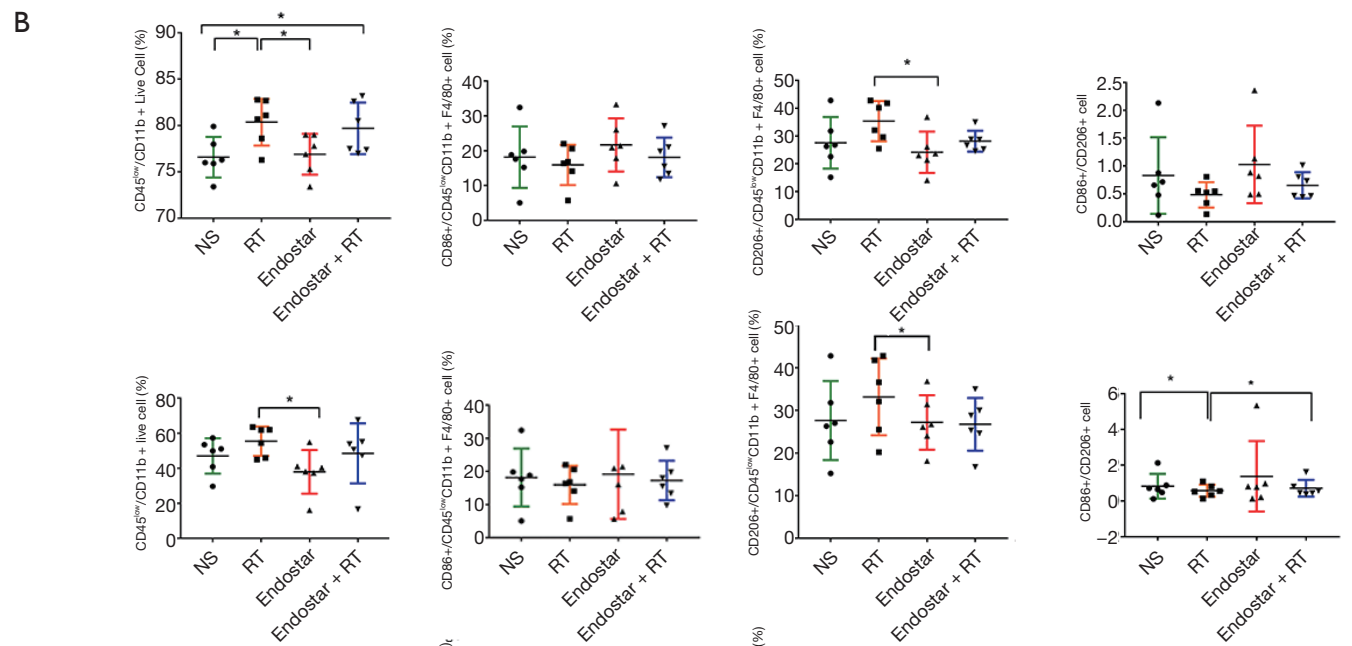

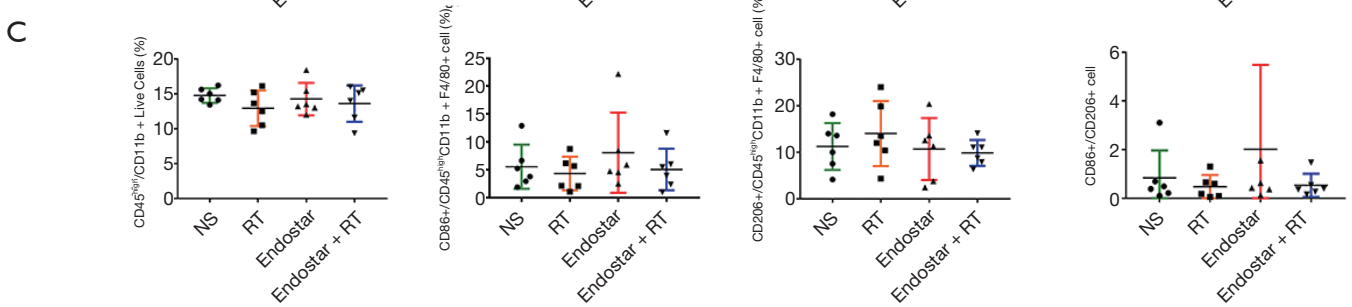

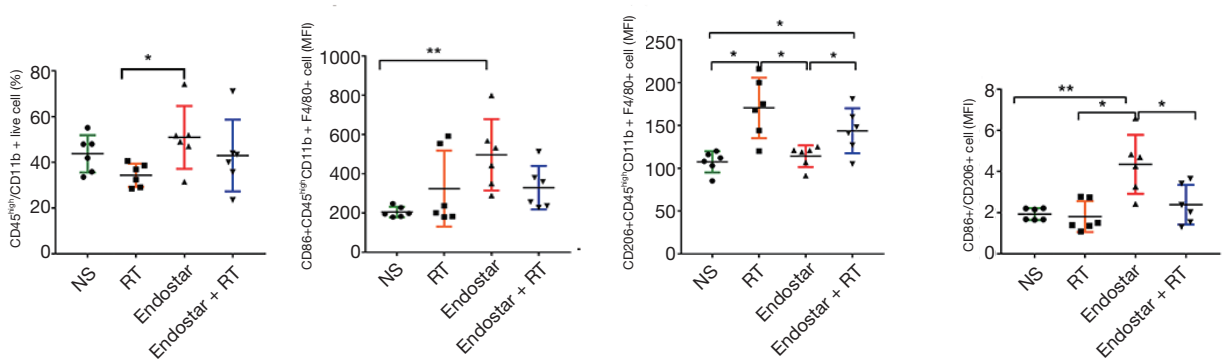

Figure 4 Endostar can reverse the changes in TAM after RT. Flow cytometry results of orthotopic transplantation model and intracarotid injection model of TAM. (A) Representative gates for microglial cells and BMDMs: microglial cells are defined as $CD45^{low}CD11b^{+}$, and bone marrow-derived macrophages are defined as $CD45^{high}CD11b^{+}$; (B) microglia, M1 phenotype microglia, M2 phenotype microglia and M1-M2 ratio in the orthotopic transplantation model (top) and intracarotid injection model (bottom) on day 14 after treatment detected by flow cytometry; (C) BMDMs, M1 phenotype BMDMs, M2 phenotype BMDMs and M1-M2 ratio in the orthotopic transplantation model (top) and intracarotid injection model (bottom) on day 14 after treatment as determined by flow cytometry. *, P<0.05; **, P<0.01. TAM, tumor-associated macrophage; RT, radiotherapy; BMDMs, bone marrow-derived macrophages.

immunosuppression. Conversely, the secretion of pro-inflammatory cytokines by M1 macrophages leads to the activation and recruitment of immune cells with antitumor abilities, including cytotoxic T cells and NK cells (39). Our research demonstrated that combining RT and ES decreased the percentage of tumor-infiltrating M2-like macrophages.

CXCL12-CXCR4 axis was previously reported to drive the accumulation of TAMs in hypoxic tumor environments and support the differentiation of monocytes toward immunosuppressive phenotypes (40). In a recent investigation, AMD3100, a CXCR antagonist through the inhibition of the CXCR4, facilitated M2-to-M1 polarization when combined with PD-1 therapy, which was otherwise reversed by elevating CXCL12 in the ovarian tumor environment (41).This novel finding stands in contrast to a previous study in a glioblastoma tumor model in which AMD3100 increased the accumulation of both M1 and M2 macrophages in the tumor. Our research found that RT-induced CXCR4, which was involved in TAM recruitment, was attenuated by ES. Therefore, we hypothesized that ES could optimize the impact of RT through blocking RT-induced CXCR4 and subsequently suppressing TAM infiltration. However, the mechanism is not clear which need more related experiment to explore the pathways in the future.

RT alone can modify the immune system, and there is sound reasoning behind the application of RT to local tumors being combined with active specific immune modulation to increase the effect of RT. Irradiation leads to the release of a substantial amount of tumor-associated antigens (TAA) from dying tumor cells, which are able to be processed by antigen-presenting cells (APCs), including dendritic cells (DCs), that can induce an immune response on surviving cells (42). Irradiation can also upregulate the many genes that elevate the presence of major histocompatibility complex class I (MHC class I) on tumor cell surfaces being absorbed by APCs. This causes the irradiated tumor cells to be more susceptible to T cell-mediated immune response (43). These responses rely partly on of $CD4^{+}$ T and $CD8^{+}$ T cells. Indeed, the reduction of $CD8^{+}$ T cells with an anti-CD8 monoclonal antibody weakens the efficacy of RT. RT elevates T-cell priming through the drainage of lymphoid tissues while exerting antitumor effects on local tumor (44).

Tumor endothelial cells are also susceptible to RT, and their destruction is a trigger for a cascade of inflammatory response. Loss of these cells also results in higher intracellular adhesion molecule (ICAM) and vasculature cell adhesion molecule (VCAM) expression, and a stronger attraction of innate immune cells (45). For example, through the downregulation and/or decluttering of ICAM1 and VCAM1, which are required for extravasation, effector cells are unable to traverse the endothelial cells (ECs)

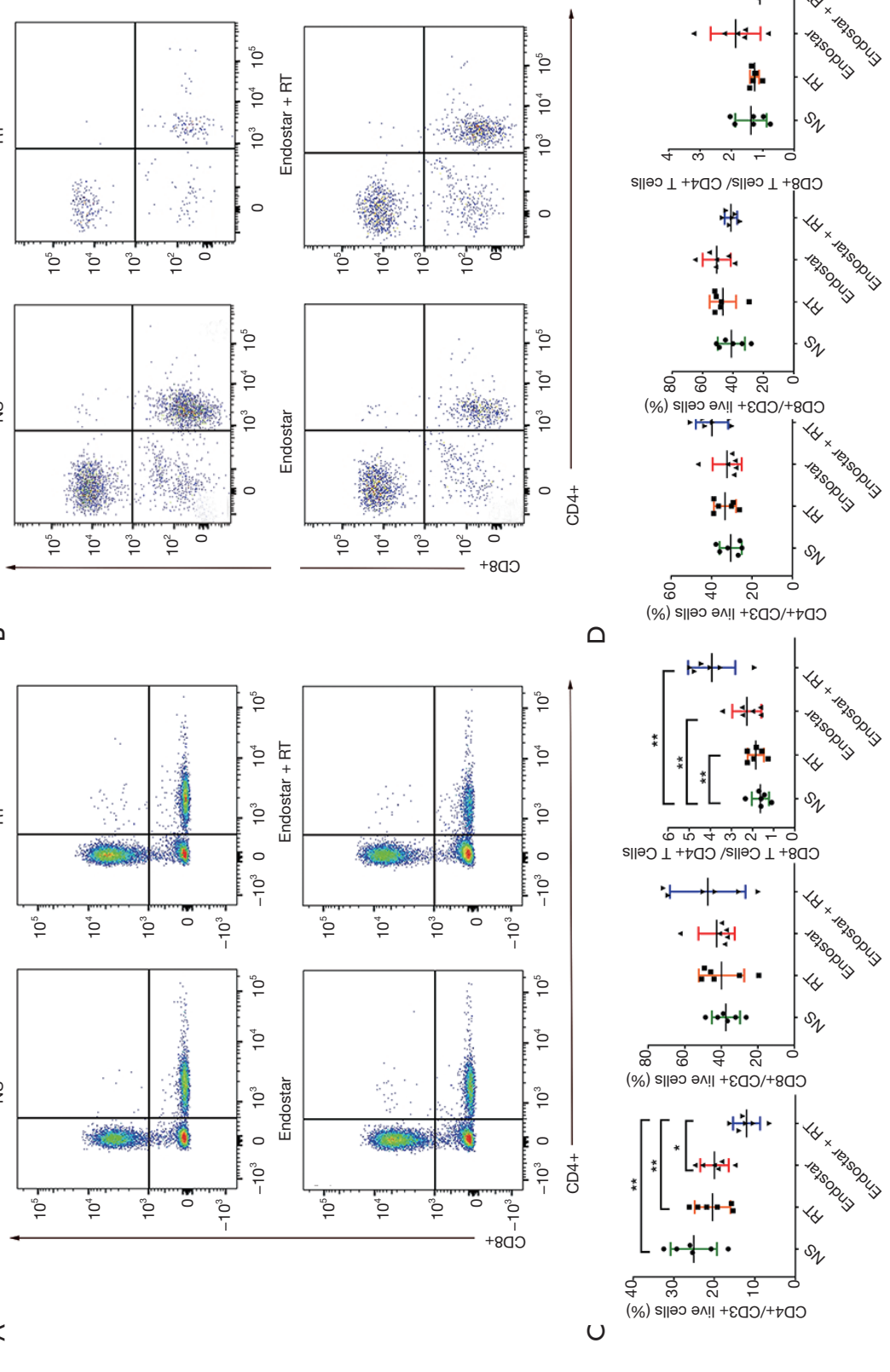

Figure 5 Combining Endostar with radiotherapy increases the proportion of CD8$^+$ T cells. Tumor tissue infiltrating T cell analysis results were shown as determined by flow cytometry. (A) Distribution of CD4$^+$ T cells and CD8$^+$ T cells in the orthotopic transplantation model on day 14 after treatment; (B) the proportion of CD4$^+$ T cells, CD8$^+$ T cells and the ratio of CD8$^+$ T cells to CD4$^+$ T cells in the orthotopic transplantation model on day 14 after treatment; (C) distribution of CD4$^+$ T cells and CD8$^+$ T cells in the intracarotid injection model on day 14 after treatment; (D) the proportion of CD4$^+$ T cells, CD8$^+$ T cells and the ratio of CD8$^+$ T cells to CD4$^+$ T cells in the intracarotid injection model on day 14 after treatment. *, $P<0.05$; **, $P<0.01$.

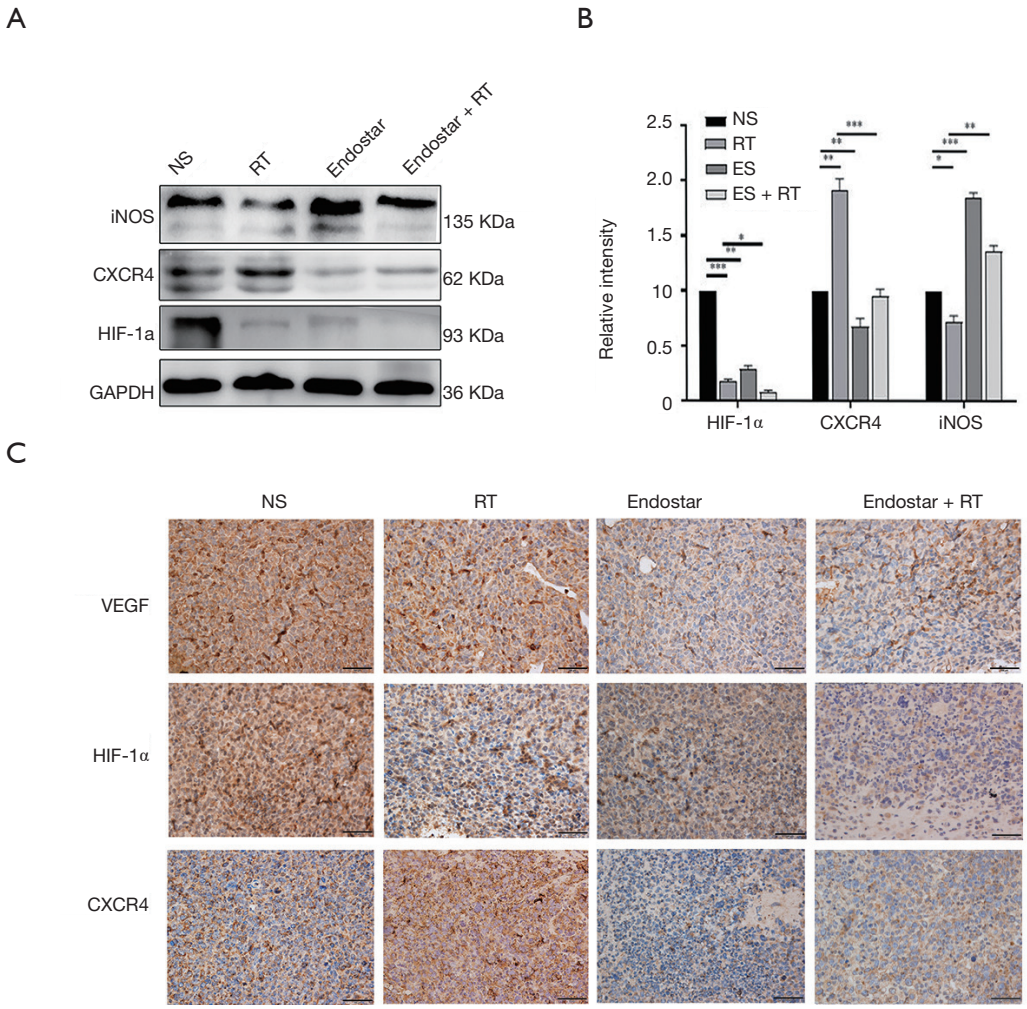

Figure 6 The expression of HIF-1α, CXCR4, and iNOS in the orthotopic transplantation model tumor tissues. (A) iNOS, CXCR4, HIF-1α were detected by WB on day 14 after treatment in the orthotopic transplantation model; (B) the results of iNOS, CXCR4, HIF-1α proteins were quantified by ImageJ and normalized to GAPDH. Protein intensity values were determined relative to the NS group (bottom). *, P<0.05; **, P<0.01; ***, P<0.001; (C) VEGF, HIF-1α, CXCR4 were detected by IHC on day 14 after treatment in the orthotopic transplantation model (scale =50 μm). HIF-1, hypoxia-inducible factor-1; VEGF, vascular endothelial growth factor; IHC, immunohistochemistry; iNOS, inducible nitric oxide synthase.

into the tumor bed. Thus, RT acts to prime the immune system against cancer cells through immunogenic cell death (ICD) but is perhaps limited by the augmented effect of suppressive immune cells.

A normalized vasculature may be able to change the tumor microenvironment from a immunosuppressive to an immunosupportive one. Atypical tumor vasculature may inhibit T-effector cells infiltrating into tumors and form a hypoxic and acidic tumor microenvironment, which is capable of upregulating PD-L1 on myeloid-derived suppressor cells (MDSCs), dendritic cells, and cancer cells. It can also restrict T effector cells, while polarizing TAMs to the immune inhibitory M2-like phenotype to suppress T-effector cell function. Hypoxia can lead to the upregulation of many immunosuppressive growth factors and cytokines (e.g., VEGF, TGFβ). Normalizing the vasculature with a suitable dose and scheduling regime of antiangiogenic treatment may homogenize the distribution of perfused tumor vessels, and thus enable the infiltration of T-effector cells while decreasing MDSC accretion (17).

Additionally, mitigating hypoxia and acidity through improved vascular perfusion can polarize TAMs to an immunostimulatory M1-like phenotype.

Our study has some limitations, as research related to pathways is still insufficient, which will be supplemented in future studies.

To conclude, ES can not only improve the tumor vascular system, but can also inhibit the recruitment of immunosuppressive cells, which can reverse the aggregation of RT-induced TAMs and other immunosuppressive cells and enhance the radiotherapeutic effect. Finally, our research lays a foundation for further exploration of the combination of antiangiogenic drugs with RT.

Acknowledgments

We want to express our sincere appreciation to the reviewers for their helpful comments on this article.
Funding: This work was supported by the Chinese Society of Clinical Oncology (CSCO), National Key R&D Program of China (Grant No 2019YFC1316205) and National Natural Science Foundation of China (No 81773233).

Footnote

Reporting Checklist: The authors have completed the ARRIVE reporting checklist. Available at http://dx.doi.org/10.21037/tlcr-20-500

Data Sharing Statement: Available at http://dx.doi.org/10.21037/tlcr-20-500

Conflicts of Interest: All authors have completed the ICMJE uniform disclosure form (available at http://dx.doi.org/10.21037/tlcr-20-500). The authors have no conflicts of interest to declare.

Ethical Statement: The authors are accountable for all aspects of the work in ensuring that questions related to the accuracy or integrity of any part of the work are appropriately investigated and resolved. All experiments were performed under a project license (license number S2326) granted by the Institutional Animal Care and Use Committee at Tongji Medical College, Huazhong University of Science and Technology, in compliance with institutional guidelines for the care and use of animals.

References

1. Bray F, Ferlay J, Soerjomataram I, et al. Global cancer statistics 2018: GLOBOCAN estimates of incidence and mortality worldwide for 36 cancers in 185 countries. CA Cancer J Clin 2018;68:394-424.
2. Nishino M, Soejima K, Mitsudomi T. Brain metastases in oncogene-driven non-small cell lung cancer. Transl Lung Cancer Res 2019;8:S298-307.
3. Addeo A, Banna GL. The crucial role of predicting brain metastases development in non-small cell lung cancer patients. J Thorac Dis 2018;10:S3305-7.
4. Khalifa J, Amini A, Popat S, et al. Brain Metastases from NSCLC: Radiation Therapy in the Era of Targeted Therapies. J Thorac Oncol 2016;11:1627-43.
5. Salem A, Asselin MC, Reymen B, et al. Targeting Hypoxia to Improve Non-Small Cell Lung Cancer Outcome. J Natl Cancer Inst 2018. doi:10.1093/jnci/djx160.
6. Gorski DH, Beckett MA, Jaskowiak NT, et al. Blockage of the vascular endothelial growth factor stress response increases the antitumor effects of ionizing radiation. Cancer Res 1999;59:3374-8.
7. Manegold PC, Paringer C, Kulka U, et al. Antiangiogenic therapy with mammalian target of rapamycin inhibitor RAD001 (Everolimus) increases radiosensitivity in solid cancer. Clin Cancer Res 2008;14:892-900.
8. Barker HE, Paget JT, Khan AA, et al. The tumour microenvironment after radiotherapy: mechanisms of resistance and recurrence. Nat Rev Cancer 2015;15:409-25.
9. Becker M, Muller CB, De Bastiani MA, et al. The prognostic impact of tumor-associated macrophages and intra-tumoral apoptosis in non-small cell lung cancer. Histol Histopathol 2014;29:21-31.
10. Sugimura K, Miyata H, Tanaka K, et al. High infiltration of tumor-associated macrophages is associated with a poor response to chemotherapy and poor prognosis of patients undergoing neoadjuvant chemotherapy for esophageal cancer. J Surg Oncol 2015;111:752-9.
11. Zhang M, He Y, Sun X, et al. A high M1/M2 ratio

of tumor-associated macrophages is associated with extended survival in ovarian cancer patients. J Ovarian Res 2014;7:19.
12. Tang X. Tumor-associated macrophages as potential diagnostic and prognostic biomarkers in breast cancer. Cancer Lett 2013;332:3-10.
13. DeNardo DG, Brennan DJ, Rexhepaj E, et al. Leukocyte complexity predicts breast cancer survival and functionally regulates response to chemotherapy. Cancer Discov 2011;1:54-67.
14. Andón FT, Digifico E, Maeda A, et al. Targeting tumor associated macrophages: The new challenge for nanomedicine. Semin Immunol 2017;34:103-13.
15. Silva VL and Al-Jamal WT. Exploiting the cancer niche: Tumor-associated macrophages and hypoxia as promising synergistic targets for nano-based therapy. J Control Release 2017;253:82-96.
16. Shang B, Cao Z, and Zhou Q. Progress in tumor vascular normalization for anticancer therapy: challenges and perspectives. Front Med 2012;6:67-78.
17. Huang Y, Yuan J, Righi E, et al. Vascular normalizing doses of antiangiogenic treatment reprogram the immunosuppressive tumor microenvironment and enhance immunotherapy. Proc Natl Acad Sci USA 2012;109:17561-6.
18. Lin MI and Sessa WC. Antiangiogenic therapy: creating a unique "window" of opportunity. Cancer Cell 2004;6:529-31.
19. Pan JH, Zhu S, Huang J, et al. Monitoring the Process of Endostar-Induced Tumor Vascular Normalization by Non-contrast Intravoxel Incoherent Motion Diffusion-Weighted MRI. Front Oncol 2018;8:524.
20. Rocha FG, Chaves KC, Chammas R, et al. Endostatin gene therapy enhances the efficacy of IL-2 in suppressing metastatic renal cell carcinoma in mice. Cancer Immunol Immunother 2010;59:1357-65.
21. Paratore S, Banna GL, D'Arrigo M, et al. CXCR4 and CXCL12 immunoreactivities differentiate primary non-small-cell lung cancer with or without brain metastases. Cancer Biomark 2011-2012;10:79-89.
22. Zhou KX, Xie LH, Peng X, et al. CXCR4 antagonist AMD3100 enhances the response of MDA-MB-231 triple-negative breast cancer cells to ionizing radiation. Cancer Lett 2018;418:196-203.
23. Jin F, Ji H, Jia C, et al. Synergistic antitumor effects of endostar in combination with oxaliplatin via inhibition of HIF and CXCR4 in the colorectal cell line SW1116. PLoS One 2012;7:e47161.
24. Wu CC, Chaudhary KR, Na YH, et al.Quality Assessment of Stereotactic Radiosurgery of a Melanoma Brain Metastases Model Using a Mouselike Phantom and the Small Animal Radiation Research Platform. Int J Radiat Oncol Biol Phys 2017;99:191-201.
25. Zhang Z, Hatori T, Nonaka H, et al. An experimental model of brain metastasis of lung carcinoma. Neuropathology 2008;28:24-8.
26. Hoves S, Ooi CH, and Wolter C., et al. Rapid activation of tumor-associated macrophages boosts preexisting tumor immunity. J Exp Med 2018;215:859-76.
27. Daphu I, Sundstrøm T, Horn S, et al. In vivo animal models for studying brain metastasis: value and limitations. Clin Exp Metastasis 2013;30:695-710.
28. Zhang C, Lowery FJ, Yu D. Intracarotid Cancer Cell Injection to Produce Mouse Models of Brain Metastasis. J Vis Exp 2017;(120):55085.
29. Pösel C, Möller K, Boltze J, et al. Isolation and Flow Cytometric Analysis of Immune Cells from the Ischemic Mouse Brain. J Vis Exp 2016;(108):53658.
30. Nair A, Bonneau RH. Stress-induced elevation of glucocorticoids increases microglia proliferation through NMDA receptor activation. Journal of Neuroimmunology 2006;171:72-85.
31. Dong P, Ma L, Liu L, et al. CD86+/CD206+, Diametrically Polarized Tumor-Associated Macrophages, Predict Hepatocellular Carcinoma Patient Prognosis. Int J Mol Sci 2016;17:320.
32. Bedi SS, Smith P, Hetz RA, et al. Immunomagnetic enrichment and flow cytometric characterization of mouse microglia. J Neurosci Methods 2013;219:176-82.
33. Folkman J. Tumor angiogenesis: therapeutic implications. N Engl J Med 1971;285:1182-6.
34. Jain RK. Normalization of tumor vasculature: an emerging concept in antiangiogenic therapy. Science 2005;307:58-62.
35. Palazón A, Aragonés J, Morales-Kastresana A, et al. Molecular pathways: hypoxia response in immune cells fighting or promoting cancer. Clin Cancer Res 2012;18:1207-13.
36. Chargari C, Clemenson C, Martins I, et al. Understanding the functions of tumor stroma in resistance to ionizing radiation: emerging targets for pharmacological modulation. Drug Resist Updat 2013;16:10-21.
37. Ngambenjawong C, Gustafson HH, and Pun SH. Progress in tumor-associated macrophage (TAM)-targeted therapeutics. Adv Drug Deliv Rev 2017;114:206-21.
38. Kozin SV, Kamoun WS, Huang Y, et al. Recruitment of myeloid but not endothelial precursor cells facilitates tumor regrowth after local irradiation. Cancer Res 2010;70:5679-85.

39. Mantovani A, Marchesi F, Malesci A, et al. Tumour-associated macrophages as treatment targets in oncology. Nat Rev Clin Oncol 2017;14:399-416.
40. Rigo A, Gottardi M, Zamo A, et al. Macrophages may promote cancer growth via a GM-CSF/HB-EGF paracrine loop that is enhanced by CXCL12. Mol Cancer 2010;9:273.
41. Zeng Y, Li B, Liang Y, et al. Dual blockade of CXCL12-CXCR4 and PD-1-PD-L1 pathways prolongs survival of ovarian tumor-bearing mice by prevention of immunosuppression in the tumor microenvironment. FASEB J 2019;33:6596-608.
42. Obeid M, Tesniere A, Ghiringhelli F, et al. Calreticulin exposure dictates the immunogenicity of cancer cell death. Nat Med 2007;13:54-61.
43. Vanpouille-Box C, Alard A, Aryankalayil MJ, et al. DNA exonuclease Trex1 regulates radiotherapy-induced tumour immunogenicity. Nat Commun 2017;8:15618.
44. Lanitis E, Irving M, and Coukos G. Targeting the tumor vasculature to enhance T cell activity. Curr Opin Immunol 2015;33:55-63.
45. Weber C, Fraemohs L, and Dejana E. The role of junctional adhesion molecules in vascular inflammation. Nat Rev Immunol 2007;7:467-77.

Cite this article as: Peng L, Wang Y, Fei S, Wei C, Tong F, Wu G, Ma H, Dong X. The effect of combining Endostar with radiotherapy on blood vessels, tumor-associated macrophages, and T cells in brain metastases of Lewis lung cancer. Transl Lung Cancer Res 2020;9(3):745-760. doi: 10.21037/tlcr-20-500

